Acc. Chem. Res. **2001,** *34,* 808−817

Using Resonance Raman Spectroscopy To Examine Vibrational Barriers to Electron Transfer and Electronic Delocalization

JOSEPH T. HUPP* AND ROBERT D. WILLIAMS
Department of Chemistry, Northwestern University, Evanston, Illinois 60208

Received August 18, 2000

ABSTRACT

A time-dependent approach to the interpretation of resonance Raman scattering intensities has been used to obtain quantitative vibrational mode displacement information from scattering intensities associated with charge-transfer excitation. The displacements and associated frequencies are the key parameters needed to understand Franck−Condon effects in electron-transfer kinetics, and to delineate in a mode-specific way the composition of vibrational reorganization energies. Application of the approach to a number of types of electron-transfer reactions is described, including symmetrical and unsymmetrical intervalence electron transfers in inorganic and organic redox systems, metal-to-ligand charge-transfer reactions, and interfacial electron-transfer reactions. Also described is how the approach can be used to elucidate mechanisms for valence delocalization in strongly interacting redox systems.

Introduction

All molecules respond to changes in charge or oxidation state by changing their geometric structures. If no bonds are severed, the changes (at least, vibrational changes[1]) tend to be small. If the oxidation-state changes involve addition or removal of nonbonding electrons—often the case in molecules containing transition metals—the changes are smaller yet. Nevertheless, the changes in structure (changes in location of the atoms within the molecule) can have enormous kinetic consequences in charge-transfer reactions: First, as shown in Figure 1a, for reactions which are not too exoergic, structural differences create vibrational barriers. The barriers, in turn, diminish charge-transfer rates—either by imposing classical thermal activation requirements (low-frequency modes) or by creating nuclear tunneling demands (high-frequency modes). Second, if charge-induced changes in solvation contribute comparatively little to the activation barrier, and if electronic communication is good, vibrational motion will define the dynamics of barrier crossing and of the overall reaction. Third, as shown in Figure 1b, for highly exoergic reactions (nested energy surfaces) structural differences enhance the overlap of reactant and product vibrational wave functions. From Fermi's golden rule, enhanced overlap *accelerates* the rate of charge transfer.[2]

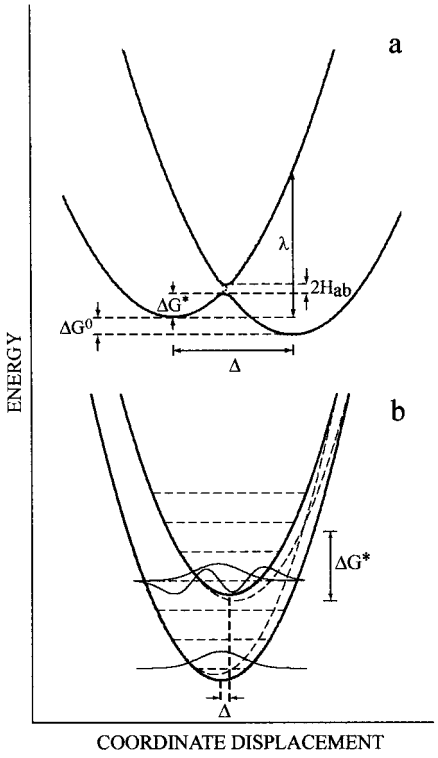

FIGURE 1. Schematic representation of free energy surfaces and their relationship to the free energy driving force ($\Delta G°$), reorganization energy (λ), classical activation free energy (ΔG^*), electronic coupling energy (H_{ab}), and vibrational mode displacement (Δ) for electron transfer in (a) the Marcus normal region and (b) the Marcus inverted region, where greater displacement leads to better vibrational overlap and faster electron transfer.

To quantify structure-change-related ET rate effects, we need two things: the vibrational frequency, ν, and the unitless normal-coordinate displacement, Δ. Note that a displacement value of 1 corresponds to one standard deviation of the Gaussian probability distribution of the ground-sate vibrational wave function. Furthermore, at least in principle, we need this information for *every* Franck−Condon active vibrational mode—that is, every vibrational mode that experiences a change in normal coordinates when an electron is transferred. In Figure 1, the normal-coordinate displacement is represented as a displacement of reactant and product curves along the horizontal axis, i.e., the traditional reaction-coordinate axis. The frequency, on the other hand, is reflected in the

Joe Hupp was born March 23, 1957, in Cuba, New York. He attended Houghton College in New York for undergraduate studies, Michigan State and Purdue for graduate studies, and the Univeristy of North Carolina for postdoctoral studies. He joined the faculty of the Chemistry Department at Northwestern University in 1986, where he is currently a Morrison Professor. His research interests include electron-transfer kinetics and dynamics, interfacial chemistry, mesoporous materials chemistry, and the parenting of twins.

Robert Williams was born February 28, 1971, in Salt Lake City, Utah, and was raised in Corona, California. After completing undergraduate work in chemistry at UCLA in 1993, he earned a Ph.D. at Northwestern University in 1998, where he contributed to the work presented here. He then moved to Princeton University as an NIH postdoctoral fellow to pursue spectroscopic studies of proteins and porphyrins with Tom Spiro. His current research interests involve applying vibrational spectroscopy to problems in electron transfer and bioinorganic chemistry.

10.1021/ar9602720 CCC: $20.00
Published on Web 08/31/2001

degree of curvature of the energy surfaces. Clearly, for weakly exoergic reactions, the bigger the mode displacement and the higher the vibrational frequency, the larger the classical activation barrier.

One way of expressing the effective magnitude of mode displacements is in terms of Marcus's vibrational reorganization energy, λ_v: the hypothetical energy cost for changing the reactant's nuclear coordinates to match those of equilibrated product; see Figure 1.[3] If the vibrations are harmonic—usually a good approximation—λ_v is given by

$$\lambda_v = 0.5\sum \Delta_k^2 \nu_k \quad (1)$$

The contribution made by a single mode, k, is

$$\lambda_{v,k} = 0.5\Delta_k^2 \nu_k \quad (2)$$

The total reorganization energy usually also includes a component due to reorientation of polar solvent molecules ($\lambda_{total} = \lambda_v + \lambda_s$).

How can the all-important displacement and reorganizational parameters be determined? One approach is to measure, typically via X-ray crystallographic or EXAFS experiments, the exact locations of all atoms in the redox reactants and all atoms in the redox products.[4] If a complete normal-coordinate analysis is available, the resulting collection of bond-length changes, Δa, can be converted to normal-coordinate displacements.[5] If the corresponding ν values are known, eqs 1 and 2 can often be used to get λ_v and $\lambda_{v,k}$. Alternatively, the needed Δ and ν values can sometimes be obtained directly from resonance Raman experiments.[6] How to do this is the focus of the next section.

The Time-Dependent Scattering Analysis

It has long been appreciated that resonance Raman experiments report on vibrational Franck–Condon activity. Recall that Raman scattering is an inelastic process entailing electronic excitation to a virtual or real molecular state (or sum of states), and a nominally instantaneous return to the ground electronic state, but in a higher or lower vibrational state (see Figure 2). The resonance Raman effect arises because electronic excitation causes a redistribution of charge which, in turn, induces normal-coordinate displacements and causes local changes in polarizability. Importantly, however, the only modes that show intensity enhancement in a resonance experiment are those displaced upon formation of the excited state.[7] Furthermore, the more they displace, the greater is the degree of enhancement.

Electronic transitions such as eq 3 are necessarily accompanied by a redistribution of charge which (a) induces normal-coordinate displacements and (b) causes local changes in polarizability. From the time-dependent

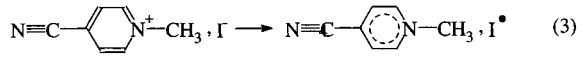

(3)

theory of Raman scattering, the relationship between the

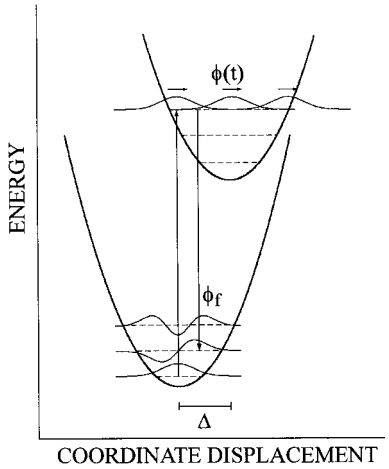

FIGURE 2. Simplified depiction of time-dependent analysis of resonance Raman scattering. The initially prepared wave packet on the upper surface evolves in time, building up overlap with a vibrational wave function on the ground electronic surface.

polarizability tensor for resonant or near-resonant scattering, α_{fi}, and the coordinate displacement, Δ_k, for mode k is given by the half-Fourier transform of the overlap of a wave packet, $\phi(t)$, moving on the upper potential energy surface (Figure 1) and a vibrational wave function, ϕ_f, on the lower surface:

$$\alpha_{fi} = \frac{2\pi i}{h}\int_0^\infty \langle\phi|\phi(t)\rangle \exp(i\omega t - \Gamma t - i\lambda_s t - \lambda_s k T t^2)\, dt \quad (4)$$

where

$$\langle\phi|\phi(t)\rangle = \prod_k \exp\left\{-\frac{\Delta_k^2}{2}[1 - \exp(-i\omega_k t)] - \frac{i\omega_k t}{2}\right\} \times [1 - \exp(-i\omega_k t)]^{n(k)} \times \frac{(-1)^{n(k)}\Delta_k^{n(k)}}{(2^{n(k)}n(k)!)^{1/2}} \exp(-iE_{00}t) \quad (5)$$

In the equations, h is Planck's constant, t is time, ω_k is 2π times the mode frequency, E_{00} is the electronic energy gap, $n(k)$ is the vibrational quantum number of the kth mode on the ground electronic surface, and Γ is a homogeneous damping term (dephasing term) which acts to kill the wave packet on the excited-state surface. Following Myers,[6a,b] two terms involving λ_s (the solvent reorganization energy for reaction 3) and the temperature have been added to eq 4. The first term (real term) acts as an inhomogeneous broadening or damping term (similar to Γ), and the second term (imaginary term) acts as an energy shift (since the solvent modes have Franck–Condon activity).

For eqs 4 and 5, the connection to experimental observables comes from the square root relationship between scattering intensities and tensor elements. In addition, as noted by Heller,[6d] the full Fourier transform of the vibrational overlap yields the absorption spectrum—which, of course, also is experimentally accessible. To determine displacements for a charge-transfer reaction, we can make use of experimentally measured relative scattering intensities, I_k, and the charge-transfer absorp-

Table 1. Experimental and Calculated Raman Cross Sections, Unitless Displacements, and Mode-Specific Reorganization Energies for Metal-to-Ligand Charge Transfer in $Ru(NH_3)_4(bpy)^{2+}$

frequency (cm^{-1})	σ_{exp} (Å/molecule)	σ_{calc}[a] (Å/molecule)	Δ[a]	$\lambda_{v,k}$[a] (kJ/mol)	Δ[b]	$\lambda_{v,k}$[b] (kJ/mol)	assignment
248	2.2×10^{-11}	2.2×10^{-11}	0.46	0.3	1.3	2.4	$\delta(H_3N-Ru-NH_3)$
376	1.3×10^{-10}	1.3×10^{-10}	0.81	1.5	2.0	9.3	ν(Ru−N(bpy))
456	2.0×10^{-11}	2.0×10^{-11}	0.27	0.2	0.65	1.1	$\nu(Ru-NH_3)$
667	2.0×10^{-10}	2.0×10^{-10}	0.62	1.5	1.2	6.2	δ(CCC) inter-ring
1027	1.1×10^{-10}	1.1×10^{-10}	0.32	0.6	0.29	0.5	ring breathing
1172	1.1×10^{-10}	1.1×10^{-10}	0.30	0.6	0.35	0.9	δ(CCH) in plane
1260	3.0×10^{-11}	3.0×10^{-11}	0.15	0.2	0.15	0.2	ν(C−C) inter-ring
1331	2.5×10^{-10}	2.5×10^{-10}	0.41	1.4	0.35	1.0	ν(C═N)
1481	4.9×10^{-10}	4.9×10^{-10}	0.55	2.7	0.52	2.4	ν(C═N)
1548	2.2×10^{-10}	2.2×10^{-10}	0.36	1.2	0.36	1.2	ν(C═C)
1605	2.4×10^{-10}	2.4×10^{-10}	0.38	1.4	0.36	1.2	ν(C═C)

[a] Time-dependent theory (previously unpublished results). [b] Savin's rule estimates; see ref 9.

tion (or emission) spectrum. Simultaneous fitting yields displacement parameters, a set of calculated relative scattering intensities, and a calculated absorption or emission spectrum. Mode-specific contributions to the vibrational reorganizational energy can be obtained from unitless normal-coordinate displacements by using eq 2, above.

Applications to Charge-Transfer Systems

Metal-to-Ligand Charge Transfer. Among the simplest and experimentally most accessible charge-transfer transitions are visible-region metal-to-ligand charge-transfer (MLCT) transitions. Some time ago we examined the Ru-(dπ)-to-bpy(π^*) transition in $Ru(NH_3)_4bpy^{2+}$ (bpy = 2,2′-bipyridine), **1**.[8] The results of a Savin's rule analysis of normal-coordinate displacements and mode-specific reorganization energies[9] are shown in Table 1, together with the results of a more sophisticated analysis involving a true time-dependent treatment of the observed absolute scattering intensities. We initially published data based only on the Savin's rule analysis, reflecting our more primitive understanding of the vibrational-reorganization problem at the beginning of our studies several years ago. Notably, results from both the primitive and more sophisticated analysis agree well with displacements derived from standard Franck−Condon analyses of low-temperature ^{3}MLCT excited-state emission spectra of closely related compounds.[10] (The tetraammine complex itself is not emissive.) Note, however, that the Raman-based analysis typically yields (a) higher precision numbers than do X-ray approaches and (b) considerably more vibrational detail than does the emission fitting approach.

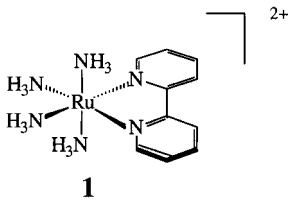

1

Interfacial Charge Transfer. In principle, the time-dependent analysis of Raman scattering intensities could be used to obtain mode specific vibrational barrier information for charge-transfer reactions occurring at electrode/solution interfaces. There are two technical problems: First, standard metal electrodes are opaque, making it difficult or impossible to obtain the charge-transfer absorption spectra needed to interpret the Raman scattering spectra. Second, the number of molecular scatterers available on a flat surface is typically orders of magnitude smaller than the number available in a solution-phase experiment, making it extremely difficult to obtain the Raman spectrum. In principle, both problems can be solved by replacing the metal electrode with medium or large band gap semiconductor particles—in the form of either high-area electrode films or extremely high surface area colloidal suspensions. The key is that the band gap opens up a region of electrode or particle transparency such that the absorption associated with the interfacial charge-transfer transition can be directly observed.

Vrachnou, Gratzel, and McEvoy have reported several examples of molecule-to-surface (TiO_2) charge-transfer absorption.[11] We carried out a resonance Raman study of one of these transitions: the ferrocyanide-to-colloidal titanium dioxide (semiconductor) charge-transfer transition shown in eq 6 and Figure 3.[12] We found that a total

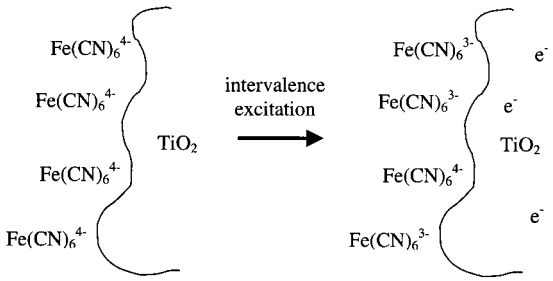

(6)

of eight vibrational modes couple to the interfacial charge transfer, the most important being a high-frequency bridging cyanide ligand stretching mode. Notably, the experiments also revealed that vibrations associated with the *semiconductor* side of the interface—in this case two Ti−O lattice stretching modes—can couple to the reaction.

The original report contained a tabulation of vibrational displacements and mode-specific reorganization energies derived from a simplified Savin's rule analysis inspired by the time-dependent treatment—again reflecting our primitive perspective at that time. Table 2 contains a revised

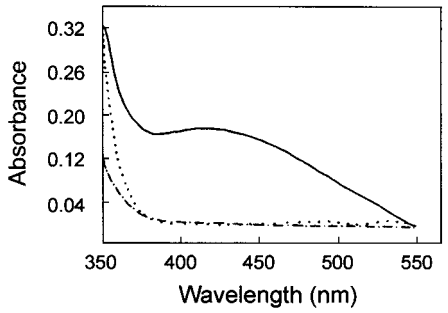

FIGURE 3. Visible-region absorption spectra of aqueous solutions of ferrocyanide (dashed line), collodial TiO_2 (dotted line), and ferrocyanide + TiO_2 (solid line). The broad absorption band centered at 420 nm corresponds to the interfacial charge-transfer transition shown in eq 6.

Table 2. Spectroscopic, Structural, and Reorganizational Parameters for Electron Transfer from $Fe(CN)_6^{4-}$ to TiO_2

mode	relative intensity	Δ	$\lambda_{v,k}$/kJ mol^{-1}	assignment
2118	20.0	1.25	16	C−N bridge
2072	6.61	0.73	5.7	C−N radial
2058	5.44	0.66	4.7	C−N terminal
720	0.27	0.34	0.4	
598	1.00	0.77	1.8	Fe−C
540	0.33	0.49	0.7	Fe−C bridge
516	1.12	0.93	2.4	Ti−O
484	0.90	0.88	2.0	Ti−O
418	0.56	0.79	1.3	Ti−O
364	0.27	0.63	0.7	Ti−N

parameter listing based on a true wave packet propagation analysis. The measurements and subsequent analysis show that, in this instance, reactant attachment to the semiconductor surface has an enormous effect upon the vibrational reorganization energy. X-ray crystallography and electrochemical EXAFS measurements, which both report on the $Fe(CN)_6^{3-/4-}$ couple in isolation, imply that just one mode rather than eight modes contribute to the barrier.[13] The measurements also imply a vibrational reorganization energy of only ca. 2−3 kJ mol^{-1}, appropriate for an outer-sphere reaction, rather than the 42 kJ mol^{-1} determined from the Raman analysis for ligand-bridge-mediated charge transfer at the semiconductor/solution interface. The Raman analysis also reveals the extensive involvement of high-frequency vibrations. The implications for the corresponding charge-transfer kinetics are that nonclassical effects (nuclear tunneling effects) will dominate. For eq 7 (below), which occurs in the inverted region, dominant nuclear tunneling should be manifest as an anomalously weak sensitivity of reaction rate to thermodynamic driving force and an insensitivity of the reaction rate to temperature (apparent activationless kinetic behavior). Notably, both kinetic effects have been seen experimentally.[14]

Other examples of interfacial charge-transfer barrier assessment via resonance Raman spectroscopy include catechol-to-TiO_2 charge transfer and quantum-confined cadmium sulfide-to-nitrobenzene charge transfer.[15,16] In the CdS/nitrobenzene case, seven modes are coupled to the charge-transfer reaction, and the largest single-mode displacement is in the Cd−S stretch. Additional experiments show, however, that the charge-transfer reaction is a highly surface-localized process with only the outermost cadmium and sulfur atoms directly participating.

Table 3. Vibrational and Reorganizational Parameters for 4-Cyano-*N*-methylpyridinium Reduction

mode frequency/ cm^{-1}	relative scattering intensity	|Δ|	$\lambda_{v,k}$/ kJ mol^{-1}	assignment
1650	1.00	1.19	14.1	ν(C=C)
1490	0.25	0.64	3.6	$\delta_{as}(CH_3)$
1290	0.20	0.64	3.1	ν(N−CH_3)
1234	0.38	0.91	6.2	νC=NCH_3)
1213	0.32	0.85	5.2	δ(C−H) (ring)
1182	0.99	1.53	16.5	(ring breathing)
844	0.42	1.32	8.9	δ(C−H) (ring)
724	0.03	0.10	0.7	γ(C−H) (ring)
678	0.08	0.69	1.9	γ(C−H) (ring)
590	0.12	0.97	3.4	γ(C=NCH_3)
551	0.15	1.16	4.4	δ(C=N=C)
416	0.19	1.69	7.1	$\gamma(CH_3)$
		total	79.9	

Outer-Sphere Charge Transfer. Many electrochemical reactions occur by outer-sphere reaction pathways. For example:

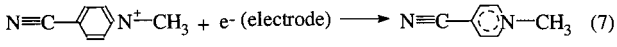

(7)

A potentially powerful way of collecting mode-specific vibrational barrier information would be to pair the electrochemical reactant with a complementary molecular or monatomic electron donor or acceptor, and then resonantly scatter photons from the resulting donor/acceptor charge-transfer transition, eq 3.[17] The challenge with donor/acceptor ion pairs and related neutral complexes is to collect meaningful Raman data despite the typically weak extinction of the charge-transfer transition. (ϵ_{max} for eq 3, for example, is only ca. 50 M^{-1} cm^{-1}.) If the charge-transfer absorbance is sufficiently weak, the observed Raman scattering can, in principle, be dominated by preresonant enhancement effects from strongly allowed transitions absorbing at higher energy, rather than by resonant charge-transfer enhancement effects. For eq 3, Raman excitation profile measurements, together with control studies with ion pairs that lack charge-transfer transitions, clearly establish that the observed scattering is dominated by the desired charge-transfer enhancement;[18] the scattering intensities, therefore, can be used in the time-dependent analysis to obtain charge-transfer barrier information. Table 3 summarizes the resonant vibrational activity observed for reaction 3 (and 7).[19] It also summarizes the displacement and mode-specific vibrational reorganizational information for reactions 3 and 7. For us, the take-home messages from the structural study were (a) that a large number of modes could contribute to the vibrational barrier for a "simple" outer-sphere electron-transfer reaction and (b) that sufficient high-frequency vibrational activity likely existed to induce significant nonclassical kinetic effects. These effects,

Table 4. Mode-Specific Kinetic Parameters for 4-Cyano-*N*-methylpyridinium Reduction

mode frequency/cm^{-1}	rate-attenuation factor[a]	sequential nuclear tunneling factor[b]
416	2.04	1.07
551	1.51	1.07
590	1.38	1.05
678	1.19	1.03
724	1.09	1.00
844	2.06	1.29
1182	2.88	2.35
1213	1.42	1.10
1234	1.48	1.32
1290	1.22	1.15
1490	1.30	1.31
1650	2.01	2.21
2250	1.20	1.40
total product	230	25

[a] Degree of electron exchange rate attenuation expected from this mode under classical conditions. [b] Degree of tunneling-based enhancement of exchange rate expected from this mode.

expressed as nuclear-tunneling-type rate enhancements, were examined by using a standard quantum mechanical, multimode electron-transfer rate treatment and are summarized in Table 4 for each of the 13 modes comprising the vibrational barrier to eq 7 under electron-exchange conditions (zero thermodynamic driving force conditions).

Unsymmetrical Mixed-Valence Systems. Unsymmetrical mixed-valence systems—especially cyanide-bridged systems—have emerged as spectacular systems for interrogating ultrafast intramolecular electron-transfer kinetics and dynamics. As suggested by the example in eq 8, intervalence excitation entails activation of precisely those modes involved in back electron transfer. Raman studies

$$(CN)_5Ru^{II}-Cu\equiv N-Ru^{III}(NH_3)_5^- \underset{k_{et}}{\overset{h\nu}{\rightleftharpoons}} (CN)_5Ru^{III}-C\equiv N-Ru^{II}(NH_3)_5^- \quad (8)$$

should yield, therefore, precisely the normal-coordinate displacements and mode-specific reorganization energies needed to understand the back ET reaction. Preliminary studies of the reaction showed that at least eight vibrational modes couple to the optical intervalence-transfer and thermal back electron-transfer processes.[20] Notably, the studies indicate Franck–Condon activity in both the donor and acceptor portions of the molecule, consistent with metal-to-metal charge transfer. The experiments also show that the single largest component of the reorganization energy comes from displacement of a bridging cyanide stretching mode—not unlike the interfacial study charge-transfer reaction discussed above. That this high-frequency mode is exceptionally Franck–Condon active is chemically reasonable. The bridging cyanide ligand is subjected to significant changes in back-bonding and in electrostatic interactions with both metal centers on account of intervalence transfer. A more quantitative description of displacements and reorganization energies requires independent information about the solvent reorganization energy and the degree of electronic coupling. Notably, the information needed to evaluate both is

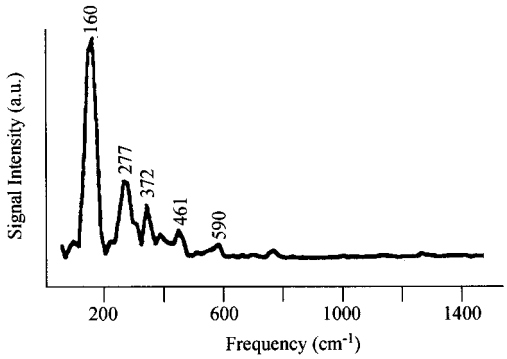

FIGURE 4. Impulsively stimulated Raman scattering spectrum of $(CN)_5Ru-CN-Ru(NH_3)_5^-$ in water as solvent. The spectrum was obtained by Fourier transforming the residuals from a fit of a transient absorbance signal for the back ET reaction shown in eq 8. Adapted from ref 23b.

becoming available from electronic Stark effect measurements for several cyanide-bridged systems.[21]

In an extension of the preliminary studies, Walker and co-workers confirmed that the remaining cyanide ligands also participate in the vibrational reorganization, albeit to a lesser extent.[22] Remarkably, however, the extent of participation proved to be adjustable on the basis of changes in the identity of the solvent. The sensitivity to solvent appeared to be associated with the propensity of these ligands to engage in varying degrees of hydrogen bonding with protic solvents.

That various metal–ligand modes are coupled to intervalence transfer has been confirmed in a strikingly direct fashion via the observation of oscillations ("quantum beats") in ultrafast transient absorbance recovery signals.[23] As shown in Figure 4 for $(CN)_5Ru-CN-Ru(NH_3)_5^-$, the frequencies extracted by Fourier transforming the residuals of transient fits are identical to those seen in Raman experiments. Further analysis shows that the oscillations result from impulsively stimulated Raman scattering during the femtosecond pump–probe experiment. A similar result has been reported by Arnett and Scherer on the basis of ultrafast pump–probe studies of the classic cyanide-bridged mixed-valent metal polymer, Prussian blue.[24]

Structures **2**–**13**, below, illustrate the molecular systems (exclusive of symmetrical dimeric systems) for which intervalence-enhanced Raman scattering data are available.[25–30] Note that the list includes an interesting trimetallic system possessing a symmetrical valence distribution in the ground state, $Fe^{II}-Pt^{IV}-Fe^{II}$, but an unsymmetrical distribution in the excited state, $Fe^{III}-Pt^{III}-Fe^{II}$ (or the energetically equivalent $Fe^{II}-Pt^{III}-Fe^{III}$). The list also includes a system for which the usual roles of metal and ligand are reversed: Diimine and dithiolate ligands serve as electron acceptor and donor, respectively, while a metal ion serves as a bridge.

Symmetrical Mixed-Valence Systems. Symmetrical mixed-valence systems are, in many respects, the simplest systems capable of displaying intramolecular electron-transfer behavior.[31] As shown in Figure 5, symmetry makes the vibrationally equilibrated redox reactants and products

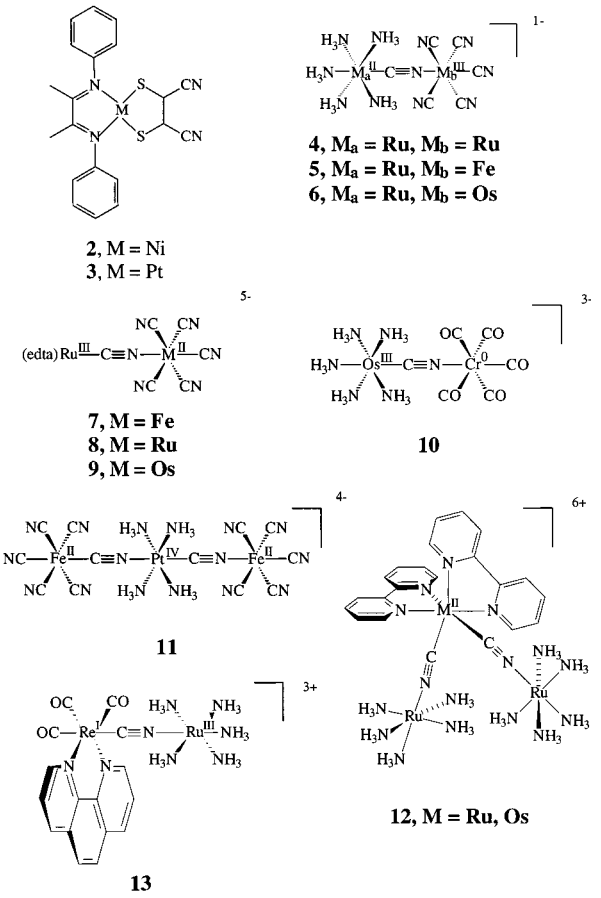

energetically equivalent and leads to particularly simple relationships between the diabatic activation free energy for thermal electron transfer, the total reorganization energy, and the optical intervalence absorption energy, i.e., $\Delta G^*(\text{dia}) = \lambda(\text{total})/4 \sim E(\text{op})/4$. The reorganization energy, in turn, is a function of normal-coordinate displacements and mode frequencies (eqs 1 and 2). Furthermore, the inherent structural symmetry of the equilibrated ET reactants and products (note that they are related as mirror images) necessarily makes the frequencies of the vibrational modes identical in the diabatic reactant and product states. We were initially surprised, therefore, to uncover significant modeling complexities in a resonance Raman study of intervalence charge transfer between covalently linked diaza donor and acceptor sites, eq 9.[32]

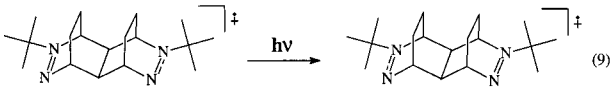

The Raman studies show that six vibrational modes couple to the intervalence transfer reaction. Consistent with the changes in nitrogen−nitrogen bond order accompanying the transfer, the most important modes are diaza stretching modes. By using relative Raman scattering intensities and the machinery associated with eqs 4 and 5, we found that the system could be modeled effectively and that a complete set of normal-coordinate displacements and mode-specific vibrational reorganization energies could be extracted. Curiously, however, the observed *absolute* Raman scattering intensities proved to be an order of magnitude smaller than expected on the basis of the structural parameters from the relative scattering analysis. The inconsistency ultimately turned out to be a diagnostic for diabatic vs adiabatic wave packet propagation. Briefly, our analyses were implemented by assuming that the wave packet propagates on a harmonic, diabatic potential energy surface (Figure 5), where here "diabatic" means a zeroth-order potential energy surface. For reaction 9, however, electronic coupling is great enough that the wave packet moves essentially exclusively on the upper, adiabatic electronic surface. (Here "adiabatic" means the surface obtained after switching on electronic coupling, i.e., the actual surface encountered in the molecular system.) Furthermore, because the avoided crossing region is exceptionally close to the Franck−Condon region for the peculiar case of symmetrical mixed-valence systems, the diabatic and adiabatic energy surfaces diverge rapidly. Because the adiabatic surface is inherently anharmonic, the wave packet motion is difficult to evaluate analytically, at least when simultaneous motion along several vibrational coordinates must be considered (i.e., the case encountered here). From an approximate treatment, however, we find that the wave packet moves much more rapidly on the adiabatic surface than on the diabatic surface. Consequently, the overlap of the packet with the pertinent ground-state vibrational wave function falls off much more rapidly in the adiabatic case, the absolute Raman scattering cross sections are much smaller, and the absolute scattering intensities are much smaller. Indeed, for reaction 9, we find that propagation on the adiabatic surface yields Raman scattering intensities that are a factor of 10 smaller than those obtained by propagating on the diabatic surface.

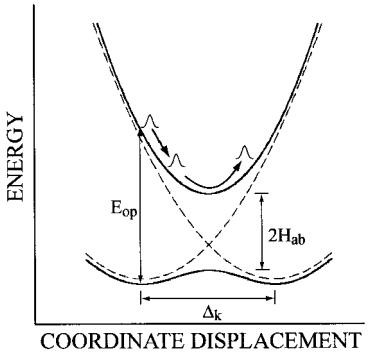

FIGURE 5. Anharmonic adiabatic (solid line) and harmonic diabatic (dashed line) potential energy surfaces for a symmetrical mixed-valence ion. Note that optical intervalence excitation launches a wave packet on the upper anharmonic surface. Note also that when $2H_{ab}$ exceeds λ (not quite the case here), the activation barrier on the ground-state surface (adiabatic surface) is lost.

The vibrational requirements for intramolecular electron transfer between directly linked ferrocenium and ferrocene moieties, **14**, have also been evaluated via intervalence excitation and Raman scattering.[33] From X-ray crystallographic studies, symmetrical ring−metal−ring stretching was known to contribute to the ET vibrational barrier.[34] We found that the Raman approach

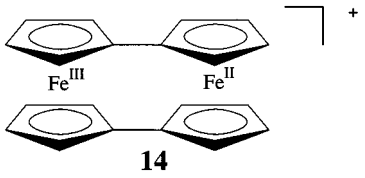

14

also did a reasonable job of capturing this information. But, it also indicated significant activity in two additional modes that were not so easily picked up via X-ray methods. We estimated that these extra modes increased the overall vibrational reorganization energy by roughly 60% and, therefore, would likely significantly modulate the corresponding electron exchange kinetics.

Applications to Electronic Structure Problems

Vibrational structural changes perform a dual function in symmetrical mixed-valence systems: They create barriers to intramolecular electron transfer, and they transiently trap electrons in local redox sites. In two-site systems, delocalization occurs when twice the electronic coupling energy, $2H_{ab}$, exceeds the total reorganizational or trapping energy (see Figure 5).[35] The archetypical example of delocalized mixed valency is the Creutz−Taube ion, **15**, where the needed coupling is engendered via good energy matching between the appropriate metal dπ orbitals and bridging-ligand π^* orbitals.[36] In a conventional electronic

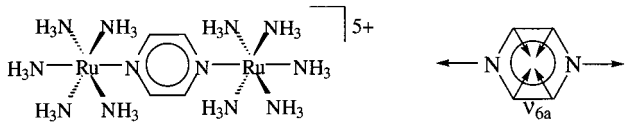

15

description, the bridge orbitals are used in an indirect or superexchange sense to mix metal-based donor and acceptor orbitals. In an alternative description, suggested some time ago by electronic structure calculations, the bridge plays a more direct role, and a three-center/three-orbital mixing and delocalization scheme is implicated.[37]

By making Raman measurements under conditions of intervalence enhancement (i.e., excitation in the extended near-infrared region), we ought to be able to discern the mechanism for delocalization. In a two-state picture, intervalence excitation leads to almost no redistribution of charge, no coupling to totally symmetric modes of the bridging ligand, and only weak coupling to other modes, such as *non*-totally symmetric modes of the bridge. In a three-state picture, on the other hand, intervalence excitation redistributes charge symmetrically from the bridging ligand to each of two metal centers—resulting in no change in molecular dipole moment but a significant change in quadrupole moment (see Scheme 1). Furthermore, the electronic excitation should couple strongly to totally symmetric bridge modes, such as the ν_{6a} mode. Resonance Raman measurements of h_4-pyrazine and d_4-pyrazine versions of the Creutz−Taube ion in the extended near-infrared region ($\lambda_{exc} = 1320$ nm; $\lambda_{max} = 1610$ nm) have

Scheme 1

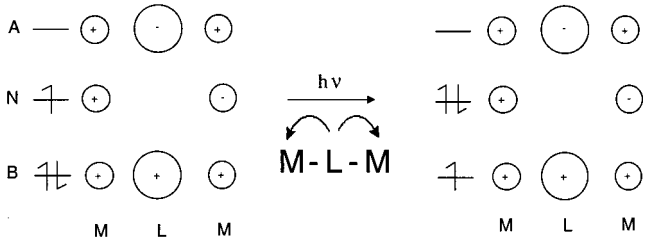

revealed a prominent totally symmetric pyrazine mode but little or no activity in non-totally symmetric modes.[38] These findings are consistent with a three-center electronic description and with direct participation of the bridging ligand in the ground-state delocalization process.

Extension of the intervalence-enhanced Raman approach to the delocalized cyclam-based bimetallic complexes, **16** and **17**, tells a similar story: The overall vibrational reorganization energies are small, but a totally symmetric vibration of the bridge dominates the scattering spectra.[39]

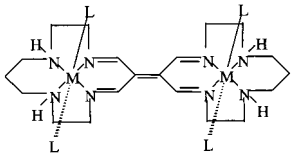

16, M = Fe, L = solvent
17, M = Ru, L = Cl

Finally, intervalence-enhanced resonance Raman spectra can provide insight into electronic interactions in lower symmetry, less strongly delocalized complexes. For example, we find that activity in the pyrazine ν_{6a} mode of compounds **18**−**23**,[40,41] as well as crown-ether complexes of **18**,[42] qualitatively correlates with the degree of ground-state valence delocalization implied by other diagnostics such as absorption bandwidths, redox asymmetry, and thermochromic behavior.[35,43]

What Is Next?

The time-dependent Raman scattering approach will undoubtedly be applied to many additional problems involving chemically interesting charge-transfer systems. There are several existing charge-transfer-related dynamic structural problems, however, that are not so easily examined in this way. These problems would seem to invite the discovery and development of improved, or altogether new, experimental probes. A partial list of candidate problems could include the following: (a) mode-specific reorganizational energetics of the solvent,[44] (b) breakdown of the Born−Oppenheimer approximation (separability of nuclear and electronic motion),[25] (c) "down stream" structural changes, i.e., changes that are initiated only after the photoexcited system moves out of the Franck−Condon region,[45] and (d) the role of *coherent* vibrational and electronic phenomena.[46]

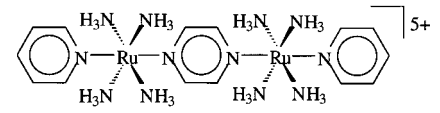

18

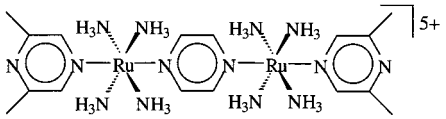

19

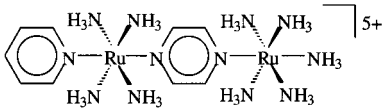

20

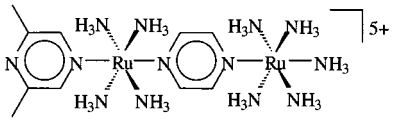

21

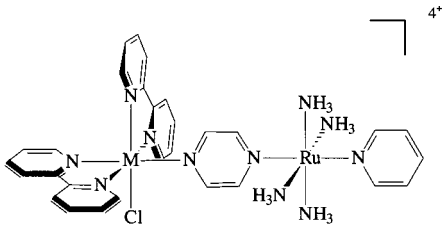

22

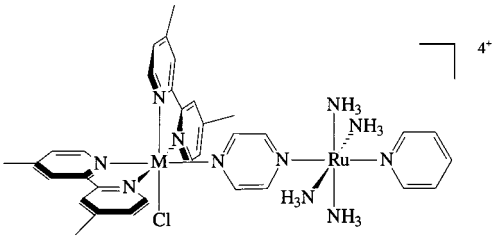

23

We gratefully acknowledge the contributions of many past and present graduate student and postdoctoral collaborators at Northwestern University, including Robert Blackbourn, Steven Doorn, Christopher Johnson, Robert Johnson, Hong Peter Lu, Timothy Marin, Vladimir Petrov, Gerald Sando, Donald Selmarten, and Frederick Vanhelmont. We also gratefully acknowledge helpful discussions with many colleagues at Northwestern and elsewhere, including Profs. Paul Barbara, Anne Kelly, Mark Ratner, Ken Spears, Gilbert Walker, and Jeff Zink. We thank the U.S. Department of Energy through the Solar Photochemistry Program of the Basic Energy Sciences Division for generous general financial support, and the Office of Naval Research specifically for support of our work involving charge transfer at interfaces.

References

(1) In principle, the changes can be vibrational, torsional (rotational), or quasi-translational (e.g., folding or unfolding of large floppy molecules or biomolecules). For a couple of reasons, we are going to limit our discussion to vibrational effects. First, even though the amplitudes of redox-induced torsional and quasi-translation motions can be large, the potentials tend to be soft, and the resulting contributions of these motions to barriers for elementary electron transfer steps tend to be small. Nevertheless, we note that both kinds of motion can profoundly affect kinetically relevant donor-site/acceptor-site electronic interactions, or can modulate overall reactivity by serving a rate-limiting "gating" function in steps preceding an elementary electron-transfer step. Second, because the potentials are soft, the characteristic frequencies of rotational and quasi-translational motions are low. This makes them difficult to detect by Raman spectroscopy, a methodology that strongly favors high-frequency modes.

(2) For a very readable review, see: Newton, M. D.; Sutin, N. Electron Transfer in Condensed Phases. *Annu. Rev. Phys. Chem.* **1984**, *35*, 487.

(3) Marcus, R. A. On the Theory of Electron-Transfer Reactions. VI. Unified Treatment for Homogeneous and Electrode Reactions. *J. Chem. Phys.* **1965**, *43*, 679.

(4) See, for example: Brunschwig, B. S.; Creutz, C.; MaCartney, D. H.; Sham, T.-K.; Sutin, N. The Role of Inner-sphere Configuration Changes in Electron-exchange Reactions of Metal Complexes. *Faraday Discuss. Chem. Soc.* **1982**, *74*, 113.

(5) Alternatively, if a local-mode approximation is acceptable, unitless coordinate displacements and bond length changes (units of distance) can be interconverted via: $|\Delta a| = (\Delta^2 h/\mu\nu b)^{1/2}$, where μ is the reduced mass of the oscillator and b is the bond degeneracy.

(6) For reviews, see: (a) Myers, A. B. Relating Absorption, Emission, and Resonance Raman-spectra with Electron-transfer Systems: Promises and Pitfalls. *Chem. Phys.* **1994**, *180*, 215. (b) Myers, A. B. Resonance Raman Intensity Analysis of Excited-State Dynamics. *Acc. Chem. Res.* **1997**, *30*, 519. (c) Zink, J. S.; Shin, K. S. Molecular Distortions in Excited Electronic States Determined from Electronic and Resonance Raman Spectroscopy. *Adv. Photochem.* **1991**, *16*, 119. (d) Heller, E. H. The Semiclassical Way to Molecular Spectroscopy. *Acc. Chem. Res.* **1981**, *14*, 368.

(7) For simplicity, we consider the case where only Albrecht A-term enhancement occurs. Thus, we ignore effects due to upper excited-state interference, including Herzberg−Teller coupling and related vibronic coupling phenomena.

(8) Doorn, S. K.; Hupp, J. T. Preresonance Raman Studies of Metal-to-Ligand Charge Transfer in $[(NH_3)_4Ru(2,2'bipyridine)]^{2+}$. *In situ* Bond-length Changes, Force Constants and Reorganization Energies. *J. Am. Chem. Soc.* **1989**, *111*, 4704.

(9) In the short-time dynamics limit, under postresonance excitation conditions, with a high-frequency mode dominating the response, the time-dependent treatment yields the following approximate relationship between scattering intensities, mode displacements, and vibrational frequencies: $I_1/I_2 = \Delta_1^2\,\nu_1^2/\Delta_2^2\,\nu_2^2$. Qualitatively, the buildup of overlap between $\phi_i(t)$ and ϕ_f in the Raman experiment (Figure 2) will occur most rapidly where the energy surface in the Franck−Condon region is steepest: Large displacements and large vibrational frequencies yield the steepest surfaces and, therefore, the highest scattering intensities. The $I/\Delta/\nu$ relationship, sometimes called Savin's rule, can also be inferred from the sum-over-states treatment. As Table 1 shows, Savin's rule typically overestimates the importance of low-frequency modes but does a fair job of describing high-frequency modes.

(10) See, for example: Caspar, J. V.; Westmoreland, T. D.; Allen, G. H.; Bradley, P. G.; Meyer, T. J.; Woodruff, W. H. Molecular and Electronic Structure in the Metal-to-Ligand Charge-Transfer Excited States of d^6 Transition-Metal Complexes in Solution. *J. Am. Chem. Soc.* **1984**, *106*, 3492−3500.

(11) Vrachnou, E,; Gratzel, M.; McEvoy, A. J. Efficient Visible-light Photoresponse Following Surface Complexation of Titanium-dioxide with Transition-metal Cyanides. *J. Electroanal. Chem.* **1989**, *258*, 193.

(12) (a) Blackbourn, R. L.; Johnson, C. S.; Hupp, T. J. Surface Intervalence Enhanced Raman Scattering from $Fe(CN)_6^{4-}$ on Colloidal Titanium Dioxide. A Mode-by-Mode Description of the Franck−Condon Barrier to Interfacial Charge Transfer. *J. Am. Chem. Soc.* **1991**, *113*, 1060. (b) Doorn, S. K.; Blackbourn, R. L.; Johnson, C. S.; Hupp, J. T. Experimental Assessment of Dynamic Structural Parameters for Homogeneous and Interfacial Charge-Transfer Reactions: Case Studies Based on Time-Dependent Raman Scattering Methods. *Electrochim. Acta* **1991**, *36*, 1775.

(13) Dewald, D. H.; Watkins, J. W.; Elder, R. C.; Heineman, W. R. Development of Extended X-Ray Absorption Fine-Structure Spectroelectrochemistry and its Application to Structural Studies of Transition-Metal Ions in Aqueous-Solution Analytical Chemistry. *Anal. Chem.* **1986**, *58*, 2968.

(14) Lu, H.; Preiskorn, J. N.; Hupp, J. T. Fast Interfacial Electron Transfer: Evidence for Inverted Region Kinetic Behavior. *J. Am. Chem. Soc.* **1993**, *115*, 4927.
(15) Selmarten, D. C. Ph.D. Thesis, Department of Chemistry, Northwestern University, 1997.
(16) For a related report, see: Yoon, D. I.; Selmarten, D. C.; Lu, H.; Liu, H.-J.; Mottley, C.; Ratner, M. A.; Hupp, J. T. Spectroscopic and Photophysical Studies of Apparent Cluster-to-Organic-Acceptor Charge Transfer in a Molecular Cadmium Sulfide Assembly. *Chem. Phys. Lett.* **1996**, *251*, 84.
(17) Other representative examples: (a) Markel, F.; Ferris, N. S.; Gould, I. R.; Myers, A. B. Mode-Specific Vibrational Reorganization Energies Accompanying Photoinduced Electron-Transfer In The Hexamethylbenzene Tetracyanoethylene Charge-Transfer Complex. *J. Am. Chem. Soc.* **1992**, *114*, 6208. (b) Britt, B. M.; McHale, J. L. Resonance Raman Study Of A Two-Chromophore System. The 2:1 Complex Of Hexamethylbenzene With Tetracyanoethylene. *Chem. Phys. Lett.* **1997**, *270*, 551.
(18) (a) Blackbourn, R. L.; Johnson, C. S.; Hupp, J. T.; Bryant, M. A.; Sobocinski, R. L.; Pemberton, J. E. A Complete Experimental Assessment of Franck−Condon Structural Effects for an Irreversible Outer-Sphere Electron-Transfer Reaction: Applications of Time-Dependent Raman Scattering Theory to the One-electron Reduction of 4-Cyano-N-methylpyridinium. *J. Phys. Chem.* **1991**, *95*, 10535. (b) Johnson, C. S. Applications of Time-Dependent Raman Scattering Theory to the One-Electron Reduction of 4-Cyano-N-methylpyridium. *J. Electrochem. Soc.* **1992**, *139*, C58.
(19) Selmarten, D. C.; Hupp, J. T. Mode-Specific Quantum Rate Effects for Interfacial Electron Transfer: Computational Case Studies Based upon 4-Cyano-*N*-methylpyridinium Reduction. *Faraday Trans.* (Electrochemistry Special Issue) **1996**, *92*, 3909.
(20) Doorn, S. J.; Hupp, J. T. Intervalence Enhanced Raman Scattering from $(NC)_5Ru-CN-Ru(NH_3)_5^-$: A Mode-by-Mode Assessment of the Franck−Condon Barrier to Intramolecular Electron Transfer. *J. Am. Chem. Soc.* **1989**, *111*, 1142.
(21) (a) Karki, L.; Lu, H. P.; Hupp, J. T. Electroabsorption Studies of Intervalence Charge Transfer in $(NC)_5Fe-CN-Os(NH_3)_5^-$: Experimental Assessment of Charge-Transfer Distance, Solvent Reorganization and Electronic Coupling Parameters. *J. Phys. Chem.* **1996**, *100*, 15637. (b) Vance, F. W.; Karki, L.; Reigle, J. K. Hupp, J. T.; Ratner, M. A. Aspects of Intervalence Charge Transfer in Cyanide-Bridged Systems: Modulated Electric Field Assessment of Distances, Polarizability Changes, and Anticipated First Hyperpolarizability Characteristics. *J. Phys. Chem. A* **1998**, *102*, 8320. (c) Vance, F. W.; Slone, R. V.; Stern, C. L.; Hupp, J. T. Comparative Absorption, Electroabsorption and Electrochemical Studies of Intervalence Electron Transfer and Electronic Coupling in Cyanide-Bridged Bimetallic Systems: Ancillary Ligand Effects. *Chem. Phys.* **2000**, *253*, 313−322. (d) Vance, F. W.; Williams, R. D.; Hupp, J. T. Electroabsorption Spectroscopy of Molecular Inorganic Compounds. *Int. Rev. Phys. Chem.* **1998**, *17*, 307.
(22) Wang, C.; Mohney, B. K.; Williams, R. D.; Petrov, V.; Hupp, J. T.; Walker, G. C. Solvent Control of Vibronic Coupling Upon Intervalence Charge-Transfer Excitation of $(CN)_5FeCNRu(NH_3)_5^-$ as Revealed by Resonance Raman and Near Infrared Absorption Spectroscopy. *J. Am. Chem. Soc.* **1998**, *120*, 5848−5949.
(23) (a) Tominaga, K.; Kliner, D. A. V.; Hupp, J. T.; Barbara, P. F. In *Ultrafast Studies on Intervalence Charge Transfer, Eight International Conference on Ultrafast Phenomena*; Martin, J. L., Migus, A., Mourou, G. A., Zewail, A. H., Eds.; Springer-Verlag: Berlin, 1993; pp 582−584. (b) Reid, P. J.; Silva, C.; Dong, Y.; Hupp, J. T.; Barbara, P. F. In *Direct Measurement of the Nuclear and Solvent Contributions to the Electron-Transfer Dynamics in Mixed Valence Metal Dimers, 9th International Conference on Ultrafast Phenomena*; Mourou, G., Zewail, A. H., Barbara, P. F., Knox, W. H., Eds.; Springer-Verlag, Berlin, 1994; p 507. (c) Reid, P. J.; Silva, C.; Barbara, P. F.; Karki, L.; Hupp, H. T. Electronic Coherence, Vibrational Coherence, and Solvent Degrees of Freedom in the Femtosecond Spectroscopy of Mixed-Valence Metal Dimers in H_2O and D_2O. *J. Phys. Chem.* **1995**, *99*, 2609.
(24) Arnett, D. C.; Vohringer, P.; Scherer, N. F. Excitation Dephasing, Product Formation and Vibrational Coherence in an Intervalence Charge-Transfer Reaction. *J. Am. Chem. Soc.* **1995**, *117*, 12262.
(25) Wootton, J. L.; Zink, J. I. Excited-State Distortions In Ligand To Ligand Charge-Transfer Excited-States of Metal Diimine Dithiolate Mixed-Ligand Complexes. *J. Phys. Chem.* **1995**, *99*, 7251.
(26) Forlano, P.; Baraldo, L. M.; Olabe, J. A.; Dellavedova, C. O. Properties of The Mixed-Valence Binuclear Complex Ion, $[NH_3)_5-Ru^{III}-NC-Os^{II}(CN)_5]$. *Inorg. Chim. Acta* **1994**, *223*, 37.
(27) Wootton, J. L.; Zink, J. I. Unusual Intensities in the Resonance Raman Spectra and Excitation Profiles of an Intervalence Metal-to-Metal Charge-Transfer Complex. *J. Am. Chem. Soc.* **1997**, *119*, 1895.
(28) Forlano, P.; Cukiernik, F. D.; Poizat, O.; Olabe, J. A. Mixed-valence Cyano-bridged complexes Containing $[M^{II}(CN)_6]^{4-}$ (M = Fe, Ru or Os) and $[Ru^{III}(edta)]^{1-}$ (edta equals ethylenedinitrilotetraacetate): Synthesis, Spectroscopic and Kinetic Characterization. *J. Chem. Soc., Dalton Trans.* **1997**, 1595.
(29) Bignozzi, C. A.; Argazzi, R.; Strouse, G. F.; Schoonover, J. R. Resonance Raman Investigation of Mixed-valence Dinuclear and Trinuclear Complexes of Ru, Os and Re. *Inorg. Chim. Acta* **1998**, *276*, 380.
(30) Hennessy, M. H.; Wu, Y.; Bocarsly, A. B.; Soos, Z. G. Electron Transfer in Symmetric Complexes: Displaced Oscillators and $[Fe(CN)_6Pt(NH_3)_4Fe(CN)_6]^{4-}$ Spectra. *J. Phys. Chem.* **1998**, *102*, 8312.
(31) For reviews, see: (a) Creutz, C. Mixed Valence Complexes of d^5-d^6 Metal Centers. *Prog. Inorg. Chem.* **1983**, *30*, 1. (b) Crutchley, R. L. Intervalence Charge Transfer and Electron Exchange Studies of Dinuclear Ruthenium Complexes. *Adv. Inorg. Chem.* **1994**, *41*, 273.
(32) Williams, R. D.; Hupp, J. T.; Ramm, M. T.; Nelson, S. F. Extended Near-Infrared Resonance Raman Investigations of an Organic Mixed-Valence System: Diazatetracyclodiene Radical Cation. *J. Phys. Chem.* **1999**, *103*, 11172−11180.
(33) Williams, R. D.; Petrov, V. I.; Lu, H. P.; Hupp, J. T. Intramolecular Electron Transfer in Biferrocene Monocation: Evaluation of Franck−Condon Effects via a Time-Dependent Analysis of Resonance Raman Scattering in the Extended Near Infrared. *J. Phys. Chem. A* **1997**, *101*, 8070−8076.
(34) Webb, R. J.; Rheingold, A. L.; Geib, S. J.; Staley, D. L.; Hendrickson, D. N. Pronounced Anion Dependence of Valence Detrapping Temperature in Mixed-Valence 1′,1‴-Disubstituted Biferocenium Salts. *Angew. Chem., Int. Ed. Engl.* **1986**, *25*, 241.
(35) Hush, N. S. Intervalence-transfer Absorption. Part 2. Theoretical Considerations and Spectroscopic Data. *Prog. Inorg. Chem.* **1967**, *8*, 391.
(36) (a) Creutz, C.; Taube, H. Binuclear Complexes of Ruthenium Ammines. *J. Am. Chem. Soc.* **1973**, *95*, 1086. (b) Best, S. P.; Clark, R. J. H.; McQueen, R. C. S.; Joss, S. The Near- and Mid-Infrared Spectrum of the Creutz-Taube Ion in Aqueous Solution: An Application of FTIR Spectroelectrochemical Techniques. *J. Am. Chem. Soc.* **1989**, *111*, 548.
(37) (a) Ondrechan, M. J.; Ko, J.; Zhang, L. T. A Model for the Optical-Absorption Spectrum of (μ-Pyrazine)decaamminediruthenium^{5+}. What Hath Creutz and Taube Wraught? *J. Am. Chem. Soc.* **1987**, *109*, 1672. (b) Piepho, S. B. Vibronic Coupling Model for the Calculation of Mixed-Valence Lineshapes: A New Look at the Creutz−Taube Ion. *J. Am. Chem. Soc.* **1990**, *112*, 4197.
(38) (a) Petrov, V.; Hupp, J. T.; Mottley, C. S.; Mann, L. C. Resonance Raman Studies in the Extended Near Infrared: Experimental Verification of a Three Site Mixing Mechanism for Valence Delocalization in the Creutz-Taube Ion. *J. Am. Chem. Soc.* **1994**, *116*, 2171−2172. (b) Lu, H.; Petrov, V.; Hupp, J. T. Intervalence Excitation of the Creutz-Taube Ion: Resonance Raman and Time Dependent Scattering Studies of Franck−Condon Effects. *Chem. Phys. Lett.* **1995**, *235*, 521−527.
(39) Karki, L.; Williams, R. D.; Hupp, J. T.; Allen, C. B.; Spreer, L. O. Electroabsorption and Related Spectroscopic Studies of Bimetallic Tetraiminoethylenedimacrocyclic Complexes: Corroboration of Valence Electron Delocalization. *Inorg. Chem.* **1998**, *37*, 2837−2840.
(40) Petrov, V.; Williams, R. D.; Hupp, J. T. Resonance Raman in the Extended Near Infrared: Experimental Time Dependent Scattering Studies of Mixed-Valence Systems. In *Proceedings of the XVth International Conference of Raman Spectroscopy*; Asher, S. A., Stein, P., Eds.; John Wiley and Sons: New York, 1996; pp 768−771.
(41) Williams, R. D. Ph.D. Thesis, Department of Chemistry, Northwestern University, 1998.
(42) (a) Dong, Y.; Hupp, J. T.; Yoon, D. I. Perturbation of the Electronic Structure of the Creutz-Taube Ion via Asymmetric Encapsulation with Macrocyclic Ether Species. *J. Am. Chem. Soc.* **1993**, *115*, 4379−4380. (b) Petrov, P.; Williams, R. D.; Hupp, J. T. Resonance Raman in the Extended Near Infrared: Experimental Time Dependent Scattering Studies of Mixed-Valence Systems. In *Proceedings of the XVth International Conference on Raman Spectroscopy*; Asher, S. A., Stein, P., Eds.; John Wiley and Sons: New York, 1996; pp 768−771. (c) Hupp, J. T.; Dong, Y. Intervalence Energy Effects Accompanying Double Crown Encapsulation of the Creutz-Taube Ion: An Interpretation Based on Three Site Mixing, *Inorg. Chem.* **1994**, *33*, 4421−4424.

(43) Hupp, J. T.; Dong, Y. Temperature Effects for Localized versus Delocalized Optical Intervalence Transitions. *J. Am. Chem. Soc.* **1993**, *115*, 6428−6429.
(44) See, for example: Castner, E. W.; Maroncelli, M. Solvent Dynamics Derived From Optical Kerr Effect, Dielectric Dispersion, and Time-resolved Stokes Shift Measurements: An Empirical Comparison. *J. Mol. Liq.* **1998**, *77*, 1−36.
(45) See, for example: Spears, K. G.; Shang, H. Models for Quantum Effects in Electron Transfer: $Co(Cp)_2^+|V(CO)_6^-$, *J. Phys. Chem.* **2000**, *104*, 2668−2680.
(46) Wynne, K.; Hochstrasser, R. M. Coherence and Adiabaticity in Ultrafast Electron Transfer. *Adv. Chem. Phys.* **1999**, *107*, 263−309.

AR9602720